Cumhuriyet Sci. J., 43(2) (2022) 221-231
DOI: https://doi.org/10.17776/csj.1086277

Cumhuriyet Science Journal

| csj.cumhuriyet.edu.tr | Founded: 2002 ISSN: 2587-2680 e-ISSN: 2587-246X Publisher: Sivas Cumhuriyet University

# Quantum Chemical Benchmark Study on Valdecoxib, a Potent and Selective Inhibitor of COX-2, and its Hydroxylated Derivative

**Sümeyya Serin** [1,a,*], **Öznur Doğan Ulu** [1,b]

[1] *Scientific and Technological Research Center, İnonu University, Malatya, Türkiye*
**Corresponding author*

**Research Article**

*History*
*Received: 11/03/2022*
*Accepted: 27/05/2022*

*Copyright*
*©2022 Faculty of Science, Sivas Cumhuriyet University*

**ABSTRACT**

In this work, quantum chemical calculations were performed on valdecoxib (VLB), a highly selective and potent COX-2 inhibitor, and its hydroxylated derivative (1H-VLB), an active metabolite. The geometry optimizations and frequency calculations were carried out by using density functional theory (DFT)/B3LYP functional with the 6-311++G (d, p) basis set. To define water phase behaviors, calculations were renewed by using universal SMD solvation model for both molecules. Structural and thermodynamic parameters, FT-IR analysis, Mulliken population analysis (MPA), frontier molecular orbital (FMO) analysis, natural bond orbital (NBO) analysis, and electrostatic surface properties were investigated in detail. Quantum chemical reactivity identifiers were calculated separately for both vacuum and water environment in order to evaluate the bioactivity tendency of both mentioned compounds. When the bioactivity of VLB and 1H-VLB molecules were compared based on quantum chemical reactivity identifiers, it was observed that the VLB molecule was more active. Moreover, drug-likeness properties of studied molecules were predicted by means of Molinspiration cheminformatics software. Molecular lipophilicity potential (MLP) maps that exhibit the accumulative lipophilic contributions of each atom in studied molecules were visualized.

***Keywords:*** Valdecoxib, DFT, Lipophilicity, NBO

[a] *sumeyya.alatas@inonu.edu.tr* *https://orcid.org/0000-0002-4637-1734* [b] *oznur.dogan@inonu.edu.tr* *https://orcid.org/0000-0002-5561-227X*

## Introduction

The increasing severity and prevalence of chronic diseases caused by inflammatory disorders pose challenges to both the health system and the economy. Therefore, there is a need for the development of environmentally friendly drugs with high efficacy and selectivity, as well as suitable toxic properties. Non-steroidal anti-inflammatory drugs (NSAIDs), commonly used in the treatment of inflammation, pain and fever inhibit cyclooxygenase (COX), also called prostaglandin synthase (PG) [1]. PGs produced from fatty acids in human organs and tissues lead symptoms such as pain, fever and redness in inflammation and injuries. COX enzymes have two different isomers called COX-1 and COX-2 [2,3]. COX-1 is involved in physical functions such as kidney function and gastrointestinal integrity, while COX-2 is responsible for proinflammatory conditions [4,5]. It was observed that the amount of PG in inflamed tissues was higher than in normal tissues [6]. The gastrointestinal side effects seen as a result of long-term use of NSAIDs necessitated the development of different drugs.

Heterocyclic compounds are widely used in organometallic chemistry, catalysis and drug chemistry for the synthesis of new and effective compounds [7,8]. Nitrogen heterocyclic compounds containing oxygen atoms have an important place in pharmaceutical chemistry. In particular, isoxazole, which has a five-membered ring containing oxygen and nitrogen atoms, attracts attention due to its biological and medicinal properties [9]. Many anti-inflammatory drugs such as flucloxacillin, dicloxacillin, cloxacillin and valdecoxib contain an isoxazole core in their structure (Figure 1).

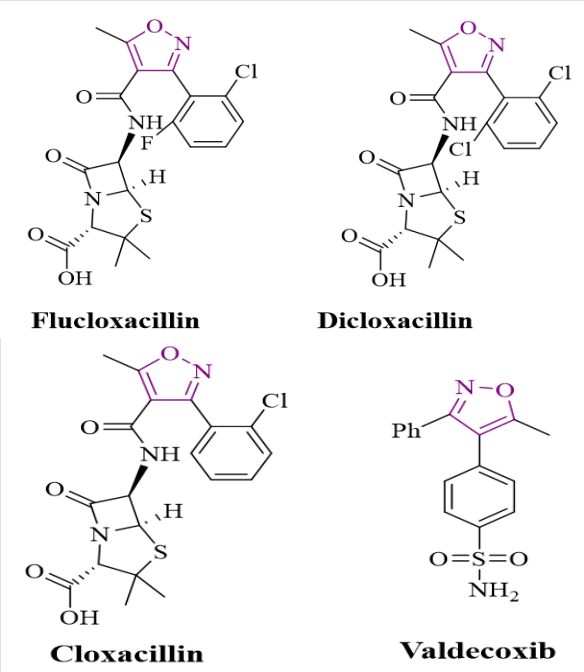


Figure 1. Structure of some drugs containing isoxazole core

Isoxazole has unsaturated double bonds and hydrogen bonds, and this unique structure makes it an important unit in the production of new compounds [9]. Valdecoxib (4-(5-methyl-3-phenyl-4-isoxazolyl) benzenesulfonamide, brand name Bextra, VLB) is an effective COX-2 inhibitor and is widely used for the treatment of pain, rheumatoid arthritis and inflammation [10]. Due to the selectivity of valdecoxib in inhibiting COX-2, different analogues were synthesized and their effects were investigated [11,12].

In general, drug design studies consist of a multi-step and time-consuming series of synthesis processes and in vivo testing steps. Then, promising compounds are investigated for their absorption, distribution, metabolism, excretion, and toxicity (ADMET) properties [13]. As the synthesis and bioactivity screenings of new drug candidates have increased significantly, the demands for the early determination of ADMET properties are also increasing. On the other hand, today, computer-aided quantum chemical calculations are frequently used to predict the values of interest for a particular molecule without performing experimental studies [14,15]. Therefore, the use of quantum chemical computational methods is very advantageous both to save time and to focus on the most promising drug candidates. Based on this information, in this study, it is aimed to perform comparative quantum chemical analysis of valdecoxib (VLB) molecule, which is a potent and selective COX-2 inhibitor, and its hydroxylated derivative (1H-VLB).

## Computational Details

The whole DFT computations of VLB and 1H-VLB were performed by using GAUSSIAN 16 software package [16]. Moreover, Gauss View 6 molecular visualization software [17] was utilized in order to visualize FMO plots and ESP maps. The geometry optimizations and frequency calculations of mentioned molecules were carried out in vacuum and also water phase by means of DFT/ B3LYP functional with 6-311++G(d,p) [18-20]. The universal SMD (Solvent Model based on Density) model was used to simulate the water phase (ε=78.4) [21]. Molinspiration Cheminformatics software [22] was used in order to calculate polar surface area (PSA), molecular volume and logPow values (logarithm of n-octanol/water partition coefficient) for lipophilicity evaluation. In addition, molecular lipophilicity potential (MLP) maps of studied molecules were visualized in Molinspiration Galaxy 3D Structure Generator v2018.01 beta [23].

In Koopmans' theorem, HOMO and LUMO energy values are associated with ionization energy (I) (Equation (1)) and electron affinity (A) (Equation (2)) [24]. In addition, kinetic stability and chemical reactivity predictions can be made by interpreting the energy gap value (ΔE) (Equation (3)) obtained from the difference of HOMO and LUMO energy values. HOMO-LUMO energy values are obtained from the molecular orbital energy levels. Therefore, if the HOMO and LUMO energies are known, parameters called quantum chemical reactivity identifiers, which ensure significant information about the activity of the molecule, can be computed. The parameters, proposed by Parr et al. [25-29] and the corresponding formulas are given below (Equations (4)-(8)):

| | | |
|---|---|---|
| Ionization Energy (I) | $I = -E_{HOMO}$ | (1) |
| Electron Affinity (A) | $A = -E_{LUMO}$ | (2) |
| Energy Gap (ΔE) | $\Delta E = E_{LUMO} - E_{HOMO}$ | (3) |
| Chemical Potential (μ) | $\mu = \frac{E_{HOMO} + E_{LUMO}}{2}$ | (4) |
| Chemical Hardness (η) | $\eta = \frac{I - A}{2}$ | (5) |
| Softness (S) | $S = \frac{1}{2\eta}$ | (6) |
| Electronegativity (χ) | $\chi = \frac{I + A}{2}$ | (7) |
| Electrophilicity index (ω) | $\omega = \frac{\mu^2}{2\eta}$ | (8) |

In another part of study, NBO analysis of mentioned molecules was explored with NBO 3.1 program integrated into Gaussian program by using B3LYP/6-311++G (d, p) level of theory. For each donor (i) and acceptor (j) NBO, the stabilization energy $E^{(2)}$ value is calculated according to the formula as follows (Equation (9)):

$$E^{(2)} = \Delta E_{ij} = qi\left[\frac{(Fij)^2}{(\varepsilon j - \varepsilon i)}\right] \quad (9)$$

$E^{(2)}$: Stabilization energy. $q_i$: Donor orbital occupancy. Fij: off diagonal Fock matrix

εi and εj: diagonal element. donor and acceptor orbital energies

## Results and Discussion

### *Molecular Structure and Vibrational Analysis*

The crystal structure of valdecoxib was acquired from the Cambridge Crystallographic Data Center (CCDC 262463). It has Pbca space group and orthorhombic crystal. The crystal structure parameters of VLB were found to be a = 12.872 (2) Å, b = 9.282 (3) Å, c = 24.761 (7) Å, and V = 2958.4 (14) Å$^3$ [30]. The optimized molecular structures of VLB and its 1-hydroxy analogue 1H-VLB with numbering and labeling scheme are represented in Figure 2. Structural parameters like bond lengths, bond angles, and dihedral angles of mentioned molecules were calculated by using B3LYP/6-311++G (d, p) level. 1H-VLB is a similar compound with VLB as structural features. Because of this, structural parameters of the 1H-VLB obtained from geometric optimization calculation checked with those of the crystal structure of the VLB. The selected experimental [30] and theoretical values are presented in Table 1.

According to Table 1, from the crystalline structure of VLB, the N2=C3 and C4=C5 bond lengths were determined as 1.317 Å and 1.347 Å, respectively. These values were calculated as 1.313 Å and 1.369 Å for VLB, 1.314 Å and 1.368 Å for 1H-VLB.

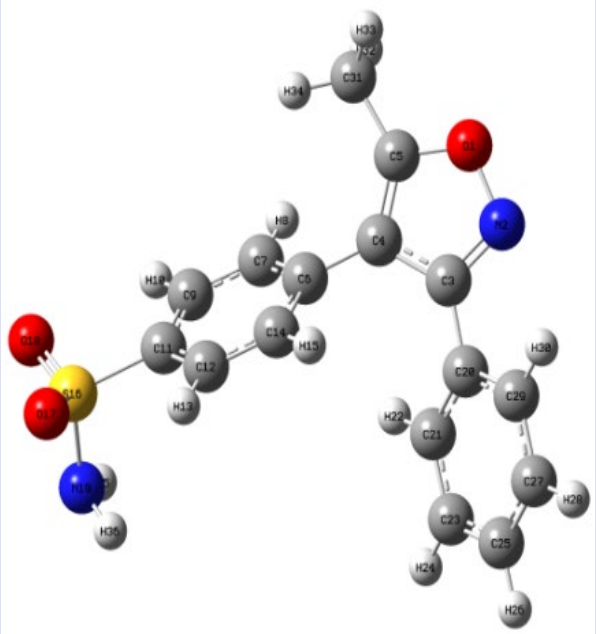

VLB

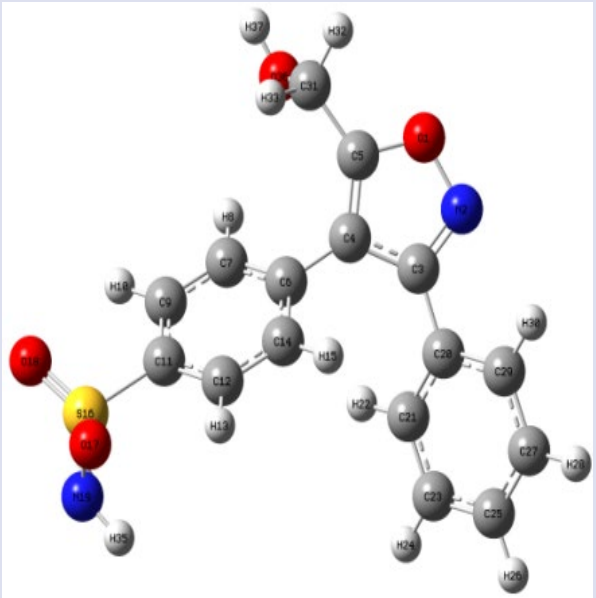

1H-VLB

Figure 2. Optimized structure of VLB and 1H-VLB

While the C3-C4 bond length was found to be 1.441 Å experimentally, it was calculated as 1.442 Å for VLB and 1H-VLB theoretically. Considering bond angles, while the bond angles of C5-O1-N2 and C3-N2-O1 were determined experimentally as 108.7° and 106.0°, they were calculated as 109.6° and 106.0° for VLB, 109.4° and 106.3° for 1H-VLB, respectively. For sulfonamide group, O17-S16-N19 and O18-S16-N19 bond angles were calculated as 105.4° and 105.3° for VLB and 105.4° for 1H-VLB. X-ray values of these angles were defined as 107.9° and 106.1° respectively. When all the bond length, bond angle, and dihedral angle values given in Table 1 are examined, it is striking that the calculation results are in good agreement with the experimental results.

Table 1. Selected geometric parameters of studied molecules

| Bond Lengths (Å) | X-ray value | VLB | 1H-VLB |
|---|---|---|---|
| O1-C5 | 1.348 | 1.346 | 1.345 |
| O1-N2 | 1.404 | 1.395 | 1.389 |
| N2-C3 | 1.317 | 1.313 | 1.314 |
| C3-C4 | 1.441 | 1.442 | 1.442 |
| C3-C20 | 1.479 | 1.477 | 1.478 |
| C4-C5 | 1.347 | 1.369 | 1.368 |
| C4-C6 | 1.482 | 1.475 | 1.473 |
| C5-C31 | 1.486 | 1.487 | 1.490 |
| C6-C14 | 1.391 | 1.404 | 1.404 |
| C6-C7 | 1.385 | 1.402 | 1.404 |
| C7-C9 | 1.382 | 1.391 | 1.392 |
| C9-C11 | 1.383 | 1.392 | 1.393 |
| C11-C12 | 1.384 | 1.394 | 1.394 |
| C11-S16 | 1.768 | 1.803 | 1.804 |
| S16-O17 | 1.424 | 1.457 | 1.457 |
| S16-O18 | 1.430 | 1.458 | 1.457 |
| S16-N19 | 1.603 | 1.681 | 1.682 |
| **Bond Angles (˚)** | | | |
| C5-O1-N2 | 108.7 | 109.6 | 109.4 |
| C3-N2-O1 | 106.0 | 106.0 | 106.3 |
| N2-C3-C4 | 110.8 | 111.2 | 111.1 |
| N2-C3-C20 | 117.5 | 119.2 | 119.1 |
| C4-C3-C20 | 131.6 | 129.6 | 129.8 |
| C5-C4-C3 | 104.0 | 103.6 | 103.3 |
| C5-C4-C6 | 125.8 | 127.1 | 126.9 |
| C3-C4-C6 | 130.2 | 129.2 | 129.8 |
| C4-C5-O1 | 110.5 | 109.6 | 110.0 |
| C4-C5-C31 | 133.9 | 133.9 | 133.2 |
| O1-C5-C31 | 115.5 | 116.5 | 116.8 |
| O17-S16-O18 | 118.5 | 123.1 | 122.9 |
| O17-S16-N19 | 107.9 | 105.4 | 105.4 |
| O18-S16-N19 | 106.1 | 105.3 | 105.4 |
| O17-S16-C11 | 107.7 | 107.4 | 107.4 |
| O18-S16-C11 | 107.8 | 107.3 | 107.4 |
| N19-S16-C11 | 108.6 | 107.5 | 107.5 |
| **Dihedral Angles (˚)** | | | |
| C5-O1-N2-C3 | -0.7 | -0.6 | -0.4 |
| O1-N2-C3-C4 | 0.4 | 0.6 | 0.2 |
| O1-N2-C3-C20 | 179.1 | 179.9 | 179.4 |
| N2-C3-C4-C5 | 0.1 | -0.4 | 0.03 |
| C20-C3-C4-C5 | -178.4 | -179.6 | -179.0 |
| N2-C3-C4-C6 | -178.0 | -177.2 | -177.3 |
| C20-C3-C4-C6 | 3.6 | 3.6 | 3.7 |
| C6-C4-C5-O1 | 177.7 | 176.9 | 177.1 |
| C3-C4-C5-C31 | -177.2 | -177.5 | -178.9 |
| S16-C11-C9-C7 | -177.7 | -179.2 | -179.2 |
| C25-C27-C29-C20 | -0.1 | 0.1 | 0.2 |

Table 2 shows the experimental and calculated vibrational frequencies of studied molecules. Experimental data for VLB were obtained from reference [31]. The vibrational modes were multiplied by 0.983 for vibrations less than 1700 $cm^{-1}$ and the larger ones were multiplied by 0.958 scale factors for B3LYP/6-311++G (d,

p) level of theory [32]. According to Table 2, while the N-H stretching vibration of VLB experimentally arised at 3377 $cm^{-1}$ and 3249 $cm^{-1}$, theoretically it was observed at 3481 $cm^{-1}$ and 3371 $cm^{-1}$ for VLB, and 3480 $cm^{-1}$ and 3370 $cm^{-1}$ for 1H-VLB. Symmetric and asymmetric stretching vibrations of S=O for VLB were calculated as 1112 $cm^{-1}$ and 1312 $cm^{-1}$, respectively. Similarly, the same vibrations were calculated as 1113 $cm^{-1}$ and 1313 $cm^{-1}$ for 1H-VLB. It is known that O-H groups give a strong absorption peak in 3700-3500 $cm^{-1}$ [33]. The characteristic O-H stretching vibration for 1H-VLB was calculated as 3667 $cm^{-1}$. In general, it was concluded that the calculated values complied with those of the experimental data.

Table 2. The experimental and calculated vibrational frequencies of VLB and 1H-VLB

| Vibration | Exp. ($cm^{-1}$) | VLB | 1H-VLB |
|---|---|---|---|
| N-H stretch | 3377 | 3481 | 3480 |
| | 3249 | 3371 | 3370 |
| N-H bend | 1544 | 1555 | 1555 |
| S=O asym stretch | 1334 | 1312 | 1313 |
| S=O sym stretch | 1150 | 1112 | 1113 |
| C-H stretch ($CH_3$) | 2929 | 2999 | 3040 |
| | 2874 | 2908 | 3031 |
| C-H stretch (Ar ring) | 3091 | 3064 | 3066 |
| O-H stretch | - | - | 3667 |
| C-H asym stretch ($CH_2$) | - | - | 2932 |
| C-H sym stretch ($CH_2$) | - | - | 2888 |

### *Thermodynamic Parameters*

The physicochemical and thermodynamic parameters such as dipole moment, total energy, enthalpy and entropy, have a crucial act in the assessment of the related chemical process in experimental and also theoretical sciences [34]. In the optimization process made with Gaussian software, the thermodynamic parameters of the chemical systems are also obtained. In this context, the results of the calculations for VLB and 1H-VLB in vacuum and water environment were given in Table 3.

It can be seen from Table 3 that the dipole moment (DM) and polarizability (α) values increase while passing from the vacuum medium to the water phase. Besides, it is seen that the heat capacity (Cv) value increases from 74.289 cal/molK to 74.310 cal/molK for VLB, and from 77.775 cal/molK to 77.976 cal/molK for 1H-VLB while going from vacuum environment into water environment. Considering the entropy (S) values, it was observed that the entropy increased with the addition of an OH group to the structure of VLB. At the same time, it is clearly seen from the Table 3 that while the entropy value is calculated as 146.971 cal/molK by decreasing for the VLB molecule in the water environment, the entropy for the 1H-VLB molecule is calculated as 155.059 cal/molK by increasing in the water environment. Also, for VLB, the ΔE values were calculated as -1351.384971 a.u. and -1351.417042 a.u. for vacuum and water phase, respectively. ΔH and ΔG values were also observed to give close results. Similarly, for 1H-VLB, ΔE values were found as -1426.611857 a. u., -1426.651455 a. u. for vacuum and water medium whereas the ΔH values were calculated as -1426.610913 a. u., -1426.650510 a. u., respectively.

Table 3. The calculated physicochemical and thermodynamic parameters of studied molecules

| | VLB | | 1H-VLB | |
|---|---|---|---|---|
| | Vacuum | Water | Vacuum | Water |
| DM (Debye) | 3.78 | 5.57 | 3.08 | 3.85 |
| ΔE (a.u.) | -1351.384971 | -1351.417042 | -1426.611857 | -1426.651455 |
| ΔH (a.u.) | -1351.384027 | -1351.416098 | -1426.610913 | -1426.650510 |
| ΔG (a.u.) | -1351.454246 | -1351.485929 | -1426.683527 | -1426.724184 |
| $\Delta E_{thermal}$ (kcal/mol) | 183.528 | 183.143 | 187.498 | 187.051 |
| Cv (cal/molK) | 74.289 | 74.310 | 77.775 | 77.976 |
| S (cal/molK) | 147.789 | 146.971 | 152.829 | 155.059 |
| α (a.u.) | 233.16 | 340.69 | 238.78 | 345.92 |
| ΔEsolv. (kj/mol) | - | -84.20 | - | -103.97 |
| ΔHsolv. (kj/mol) | - | -84.20 | - | -103.96 |
| ΔGsolv. (kj/mol) | - | -83.18 | - | -106.75 |

### *HOMO-LUMO Analysis and Quantum Chemical Reactivity Identifiers*

HOMOs (Highest Occupied Molecular Orbital) and LUMOs (Lowest Unoccupied Molecular Orbital), known as frontier molecular orbitals, play a substantial role in chemical reactivity as well as in UV-Vis absorption spectra and optical properties [35]. Besides, HOMO-LUMO diagrams which provide a visual advantage for the interpretation of the electronic properties of a wide variety of molecular systems in many fields are frequently used in computational chemistry [36]. The HOMO-LUMO diagrams of VLB and 1H-VLB computed at B3LYP/6-311++G (d, p) level of theory corresponding to the vacuum and water medium are shown in the Figure 3 and Figure 4. For both molecules, it is clear that HOMO is spread over almost the entire molecule for not only gas phase but also water phase. Similarly, for both molecules, it is seen that LUMOs are predominantly concentrated on the benzenesulfonamide and isoxazole ring.

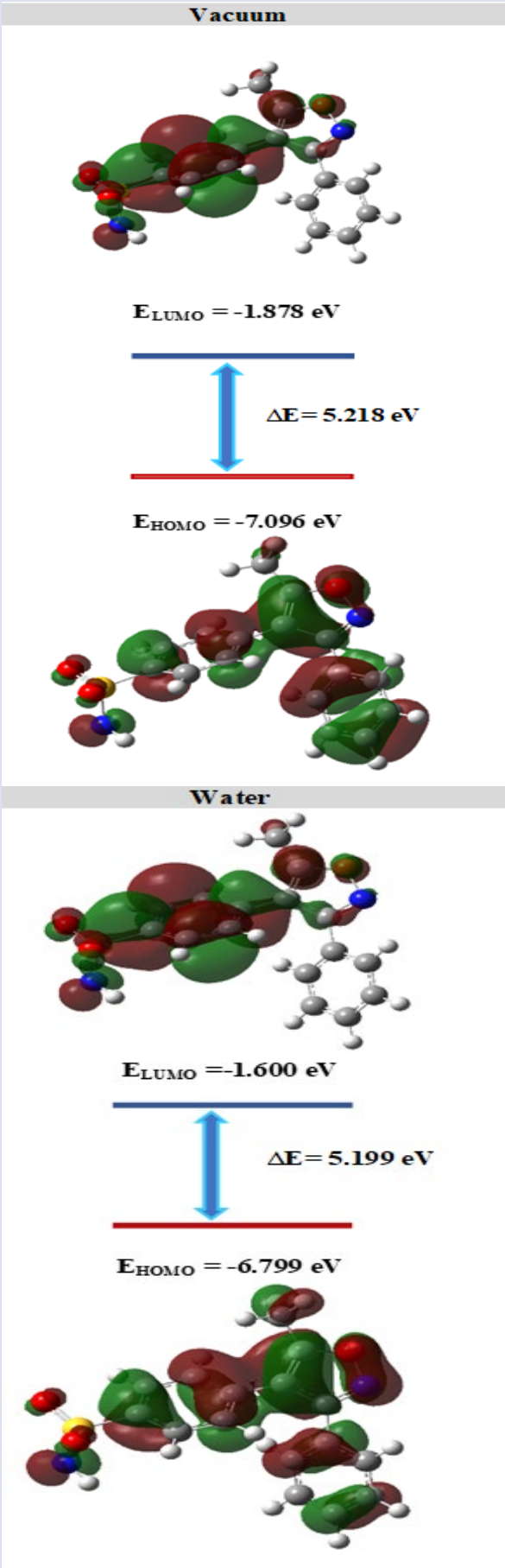


Figure 3. HOMO-LUMO plots of VLB

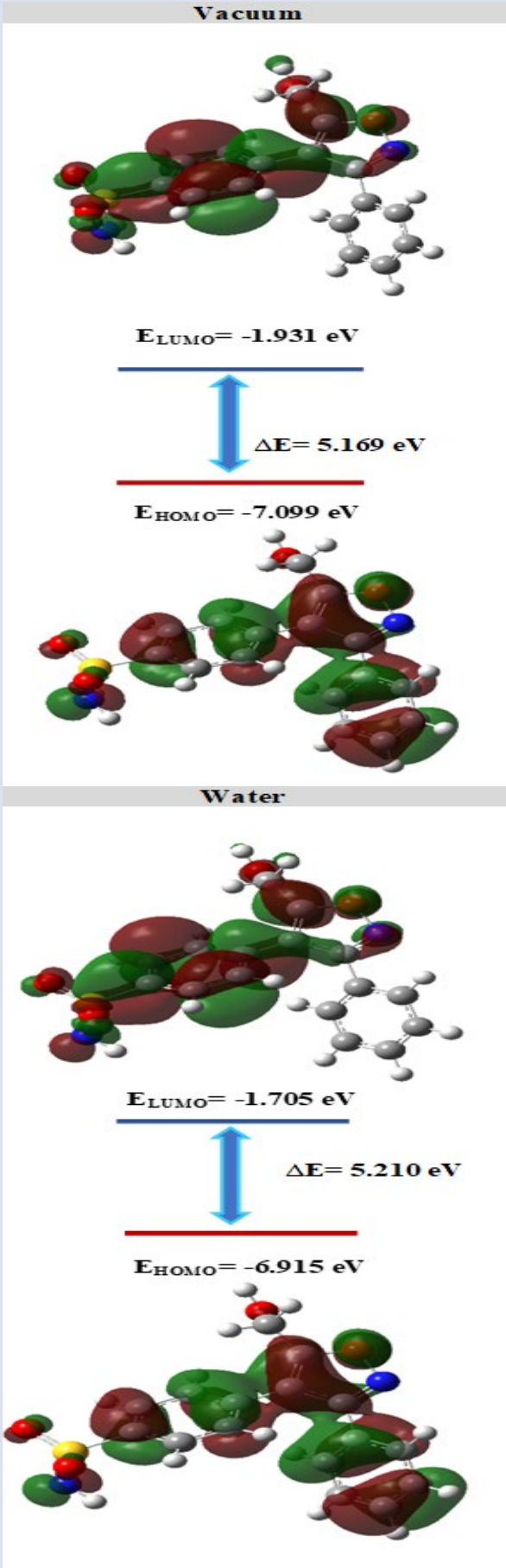


Figure 4. HOMO-LUMO plots of 1H-VLB

The calculated quantum chemical parameters for the vacuum and water environment of the studied molecules are listed in Table 4. According to Table 4, energy gap values were calculated as 5.218 eV and 5.199 eV for VLB in vacuum and water environment and as 5.169 eV and 5.210 eV for 1H-VLB, respectively. With the help of calculated quantum chemical reactivity identifiers of a given molecule, important information can be obtained about the general trend of its biological activity. There are several studies in the literature to explain the stability and reactivity of molecules using quantum chemical computational methods. [37,38]. In this context, if we compare the bioactivity of VLB and 1H-VLB molecules in water based on quantum chemical reactivity identifiers, it is concluded that VLB molecule is more active for all parameters except ELUMO. The results obtained here support the conclusion that the VLB molecule has an excellent oral activity in animal models used to develop NSAIDs compared to the 1H-VLB molecule [12].

Table 4. Calculated quantum chemical parameters of studied molecules in eV (S: $eV^{-1}$)

| | | $E_{HOMO}$ | $E_{LUMO}$ | ΔE | η | S | μ | χ | ω |
|---|---|---|---|---|---|---|---|---|---|
| Vacuum | VLB | -7.096 | -1.878 | 5.218 | 2.609 | 0.192 | -4.487 | 4.487 | 3.859 |
| | 1H-VLB | -7.099 | -1.931 | 5.169 | 2.584 | 0.193 | -4.515 | 4.515 | 3.944 |
| Water | VLB | -6.799 | -1.600 | 5.199 | 2.599 | 0.192 | -4.200 | 4.200 | 3.393 |
| | 1H-VLB | -6.915 | -1.705 | 5.210 | 2.605 | 0.192 | -4.310 | 4.310 | 3.566 |

### *Molinspiration Analysis*

Rapid and accurate prediction of molecular transport properties is one of the principal agents speeding up the drug discovery and development process [39]. The parameter commonly used for this purpose is the n-octanol/water partition coefficient, which expresses lipophilicity. However, in recent years, several different descriptors have been introduced to predict the absorption, distribution, metabolism and excretion (ADME) characteristics of drug candidates. In particular, the limiting parameters known as Lipinski's rule of five have been very popular [40]. On the other hand, in this study, polar surface area (PSA) and molecular lipophilicity potential (MLP) descriptors, which are very useful parameters, were calculated separately for VLB and 1H-VLB. Physicochemical parameter computations were performed by means of Molinspiration cheminformatics software in order to evaluate the structure-activity relationships for VLB and its hydroxy analogue. The results are listed in Table 5. According to the Table 5, the numbers of hydrogen bond donors and acceptors increase with the addition of a hydroxy group to the VLB molecule. Similarly, the molecular volume and polar surface area values were calculated as 263.55 $Å^3$ and 86.20 $Å^2$ for VLB, respectively, and increased to 271.81 $Å^3$ and 106.42 $Å^2$ for 1H-VLB.

Table 5. Molinspiration computations of molecular properties of studied molecules

| | VLB | 1H-VLB |
|---|---|---|
| PSA ($Å^2$) | 86.20 | 106.42 |
| Volume ($Å^3$) | 263.55 | 271.81 |
| $LogP_{calc}$ | 2.73 | 2.09 |
| Formula weight (g/mol) | 314.37 | 330.37 |
| Number of rotatable bonds | 3 | 4 |
| Number of H-bond donors | 2 | 3 |
| Number of H-bond acceptors | 5 | 6 |

Furthermore, as a visual identifier of lipophilicity, the molecular lipophilicity potential (MLP) maps of studied molecules were illustrated in Figure 5. The MLP map defines the 3D distribution of hydrophilic/lipophilic potential on the molecular surface via color codes. 3D CPK images were used to make the MLP map more understandable in Figure 5.

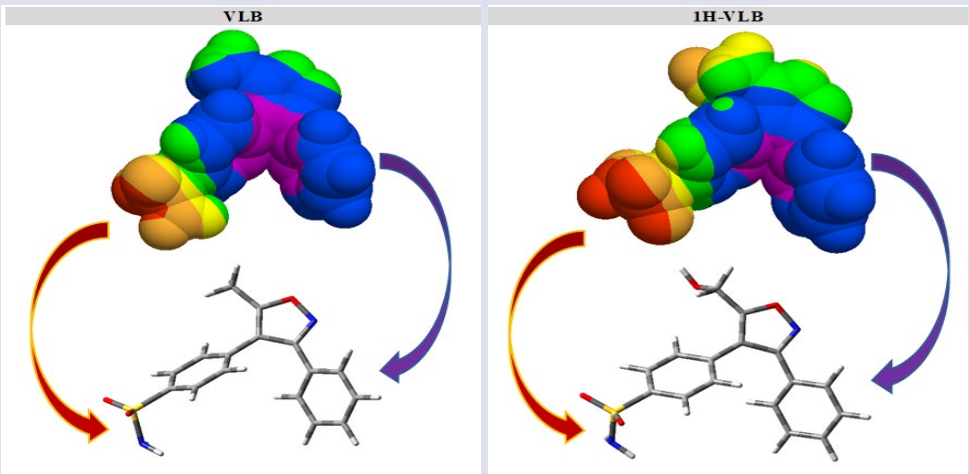


Figure 5. 3D CPK view of MLP maps of VLB and 1H-VLB

Orange and red regions represent hydrophilic surfaces, while regions coded with purple and blue indicate the most lipophilic surfaces. Additionally, regions coded in yellow and green indicate intermediate lipophilic surfaces. As can be seen from the MLP maps, the blue and purple regions in the VLB molecule are more intense than in 1H-VLB.On the other hand, in 1H-VLB molecule, it is observed that the area of the red and orange regions increases with the addition of the -OH group. Based on this information, it is concluded that the VLB molecule is more lipophilic than 1H-VLB. As can be seen from Table 5, while the $logP_{ow}$ value was calculated as 2.73 for VLB, it was calculated as 2.09 for 1H-VLB.Molinspiration calculation results indicate that phenyl rings of VLB and 1H-VLB support predominantly lipophilic interactions, and sulfonamide and hydroxyl groups support hydrophilic interactions.

### *Mulliken Population Analysis*

The total atomic charges of VLB and 1H-VLB obtained by Mulliken [41] population analysis with B3LYP/ 6-311++G (d, p) level of theory were presented in Table 6 and Figure 6. Natural charges [42] are given in NBO analysis section. According to Mulliken population analysis, there are both positively charged and negatively charged carbon atoms in both structures. While the charges of C3 bound to N2 and C5 bound to O1 atoms were calculated as 0.168e and -0.212e for VLB, they were calculated as 0.504e and 0.106e for 1H-VLB, respectively. C6 and C20 atoms were found to have the highest positive charge of 0.578e and 1.362e for VLB, 0.550e and 1.402e for 1H-VLB, respectively. It was determined that while the charges of O1 and S16 atoms from O, S, and N heteroatoms in the structures were positive, N2, N19, O17, O18 and O36 atoms were negatively charged. Furthermore, it is clear from the Mulliken histogram that all hydrogens are positively charged. It was determined that H35 and H36 atoms attached to N19 in the VLB molecule have the highest positive value (0.286e and 0.287e) due to the electron withdrawing property of the nitrogen atom. The same is true for H34 and H35 atoms (0.286e and 0.287e) in the 1H-VLB molecule.

Table 6. Mulliken atomic charge values of VLB and 1H-VLB

| Atom | VLB | 1H-VLB | Atom | VLB | 1H-VLB |
|---|---|---|---|---|---|
| O1 | 0.300 | 0.319 | C20 | 1.362 | 1.402 |
| N2 | -0.459 | -0.476 | C21 | -0.406 | -0.434 |
| C3 | 0.168 | 0.504 | H22 | 0.167 | 0.168 |
| C4 | -0.315 | -0.853 | C23 | -0.275 | -0.282 |
| C5 | -0.212 | 0.106 | H24 | 0.182 | 0.185 |
| C6 | 0.578 | 0.550 | C25 | -0.356 | -0.359 |
| C7 | -0.477 | -0.594 | H26 | 0.154 | 0.154 |
| H8 | 0.208 | 0.275 | C27 | -0.294 | -0.316 |
| C9 | -0.257 | -0.224 | H28 | 0.181 | 0.183 |
| H10 | 0.265 | 0.259 | C29 | -0.049 | 0.067 |
| C11 | -0.214 | -0.200 | H30 | 0.218 | 0.220 |
| C12 | -0.394 | -0.350 | C31 | -0.614 | -0.676 |
| H13 | 0.261 | 0.261 | H32 | 0.199 | 0.189 |
| C14 | -0.553 | -0.584 | H33 | 0.181 | 0.166 |
| H15 | 0.194 | 0.192 | H34 | 0.154 | 0.286 |
| S16 | 0.201 | 0.217 | H35 | 0.286 | 0.287 |
| O17 | -0.178 | -0.181 | H36 | 0.287 | - |
| O18 | -0.188 | -0.182 | O36 | - | -0.228 |
| N19 | -0.301 | -0.303 | H37 | - | 0.252 |

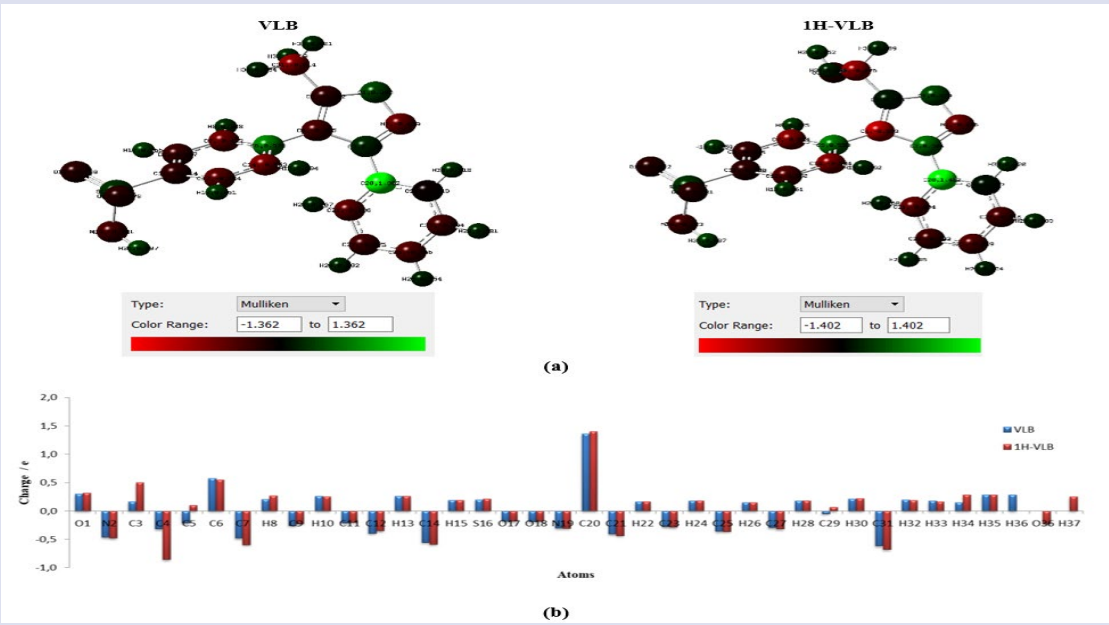


Figure 6. (a) Mulliken atomic charge distributions and (b) Mulliken histogram of VLB and 1H-VLB

### *Natural Bond Orbital (NBO) Analysis*

The natural bond orbital (NBO) analysis ensures detailed information about interactions between donor and acceptor orbitals. In order to estimate stabilization energies ($E^{(2)}$) , second order Fock matrix is utilized [43, 44]. The stabilization energy, $E^{(2)}$, expresses the intensity of electron delocalization between the bonding (BD) or lone pair (LP) orbitals and anti-bonding (BD*) orbitals. The higher $E^{(2)}$ value means that the interaction between the donor and acceptor orbitals is more intensive.

The calculated natural charges and effective valence electron configurations (NEC) for each atom except hydrogens of VLB and 1H-VLB are summarized in Table 7. Additionally, the second order perturbation theory results of Fock matrix in NBO basis for studied molecules are represented in Table 8 and Table 9.

Table 7. Summary of natural charges and natural electron configurations

| VLB | | | 1H-VLB | | |
|---|---|---|---|---|---|
| Atom | Natural Charge | Natural Electron Configuration | Atom | Natural Charge | Natural Electron Configuration |
| O1 | -0.32474 | [core]$2S^{1.62}2p^{4.68}3p^{0.01}3d^{0.01}$ | O1 | -0.31100 | [core]$2S^{1.62}2p^{4.67}3p^{0.01}3d^{0.01}$ |
| N2 | -0.13784 | [core]$2S^{1.48}2p^{3.63}3d^{0.01}4p^{0.01}$ | N2 | -0.12899 | [core]$2S^{1.48}2p^{3.62}3d^{0.01}4p^{0.01}$ |
| C3 | 0.16930 | [core]$2S^{0.84}2p^{2.96}3d^{0.01}4p^{0.02}$ | C3 | 0.16607 | [core]$2S^{0.84}2p^{2.96}3d^{0.01}4p^{0.02}$ |
| C4 | -0.18434 | [core]$2S^{0.86}2p^{3.30}3p^{0.01}4p^{0.01}$ | C4 | -0.14774 | [core]$2S^{0.86}2p^{3.26}4p^{0.01}$ |
| C5 | 0.38330 | [core]$2S^{0.85}2p^{2.75}3p^{0.01}3d^{0.01}4p^{0.01}$ | C5 | 0.35263 | [core]$2S^{0.85}2p^{2.77}3d^{0.01}4p^{0.02}$ |
| C6 | -0.02421 | [core]$2S^{0.86}2p^{3.15}3p^{0.01}$ | C6 | -0.04373 | [core]$2S^{0.87}2p^{3.15}4p^{0.01}$ |
| C7 | -0.18976 | [core]$2S^{0.94}2p^{3.23}4p^{0.01}$ | C7 | -0.18641 | [core]$2S^{0.95}2p^{3.22}4p^{0.01}$ |
| C9 | -0.19018 | [core]$2S^{0.95}2p^{3.22}4p^{0.01}$ | C9 | -0.19026 | [core]$2S^{0.95}2p^{3.22}4p^{0.01}$ |
| C11 | -0.28008 | [core]$2S^{0.98}2p^{3.27}4p^{0.02}$ | C11 | -0.27900 | [core]$2S^{0.98}2p^{3.27}4p^{0.02}$ |
| C12 | -0.18841 | [core]$2S^{0.95}2p^{3.22}4p^{0.01}$ | C12 | -0.19116 | [core]$2S^{0.95}2p^{3.23}4p^{0.01}$ |
| C14 | -0.17535 | [core]$2S^{0.94}2p^{3.22}4p^{0.01}$ | C14 | -0.17300 | [core]$2S^{0.94}2p^{3.22}4p^{0.01}$ |
| S16 | 2.19601 | [core]$3S^{1.05}3p^{2.54}3d^{0.17}5p^{0.04}$ | S16 | 2.19544 | [core]$3S^{1.05}3p^{2.54}3d^{0.17}5p^{0.04}$ |
| O17 | -0.90874 | [core]$2S^{1.83}2p^{5.07}3d^{0.01}$ | O17 | -0.90975 | [core]$2S^{1.83}2p^{5.07}3d^{0.01}$ |
| O18 | -0.91026 | [core]$2S^{1.83}2p^{5.07}3d^{0.01}$ | O18 | -0.91029 | [core]$2S^{1.83}2p^{5.07}3d^{0.01}$ |
| N19 | -1.02481 | [core]$2S^{1.50}2p^{4.50}3p^{0.01}$ | N19 | -1.02457 | [core]$2S^{1.50}2p^{4.50}3p^{0.01}$ |
| C20 | -0.08117 | [core]$2S^{0.86}2p^{3.20}4p^{0.01}$ | C20 | -0.08331 | [core]$2S^{0.86}2p^{3.20}4p^{0.01}$ |
| C21 | -0.17228 | [core]$2S^{0.93}2p^{3.23}4p^{0.01}$ | C21 | -0.17060 | [core]$2S^{0.93}2p^{3.22}4p^{0.01}$ |
| C23 | -0.20539 | [core]$2S^{0.95}2p^{3.24}4p^{0.01}$ | C23 | -0.20512 | [core]$2S^{0.95}2p^{3.23}4p^{0.01}$ |
| C25 | -0.19220 | [core]$2S^{0.95}2p^{3.22}4p^{0.01}$ | C25 | -0.19142 | [core]$2S^{0.95}2p^{3.22}4p^{0.01}$ |
| C27 | -0.20359 | [core]$2S^{0.95}2p^{3.23}4p^{0.01}$ | C27 | -0.20362 | [core]$2S^{0.95}2p^{3.23}4p^{0.01}$ |
| C29 | -0.15533 | [core]$2S^{0.93}2p^{3.21}4p^{0.01}$ | C29 | -0.15601 | [core]$2S^{0.93}2p^{3.21}4p^{0.01}$ |
| C31 | -0.62508 | [core]$2S^{1.09}2p^{3.53}$ | C31 | -0.07752 | [core]$2S^{1.01}2p^{3.05}3p^{0.01}4S^{0.01}3d^{0.01}$ |
| | | | O36 | -0.72760 | [core]$2S^{1.69}2p^{5.02}3p^{0.01}$ |

Table 8. Second-order perturbation theory results of Fock matrix in NBO basis for VLB

| Donor(i) | $ED_i/e$ | Acceptor(j) | $ED_j/e$ | $E^{(2)}$ kcal/mol | E(j)-E(i)/a.u | F(i.j)/a.u |
|---|---|---|---|---|---|---|
| π N2-C3 | 1.90673 | π* C4-C5 | 0.28248 | 8.27 | 0.36 | 0.051 |
| | | π* C20-C21 | 0.36957 | 5.20 | 0.36 | 0.042 |
| π C4-C5 | 1.78536 | π* N2-C3 | 0.31719 | 26.03 | 0.29 | 0.080 |
| | | π* C6-C7 | 0.35208 | 6.74 | 0.30 | 0.041 |
| π C6-C7 | 1.63703 | π* C9-C11 | 0.38412 | 24.03 | 0.27 | 0.072 |
| | | π* C12-C14 | 0.29223 | 18.31 | 0.28 | 0.065 |
| π C9-C11 | 1.68575 | π* C6-C7 | 0.35208 | 16.70 | 0.30 | 0.064 |
| | | π* C12-C14 | 0.29223 | 21.20 | 0.30 | 0.071 |
| σ S16-O18 | 1.98735 | π* C23-C25 | 0.33092 | 9.41 | 0.61 | 0.074 |
| σ C20-C21 | 1.96888 | π* C23-C25 | 0.33092 | 13.34 | 0.33 | 0.064 |
| π C23-C25 | 1.65558 | π* C20-C21 | 0.36957 | 21.01 | 0.28 | 0.069 |
| π C27-C29 | 1.65536 | π* C20-C21 | 0.36957 | 20.37 | 0.28 | 0.068 |
| LP (2) O1 | 1.70777 | π* N2-C3 | 0.31719 | 16.36 | 0.42 | 0.074 |
| LP (2) O17 | 1.81964 | σ* C11-S16 | 0.20565 | 15.54 | 0.44 | 0.074 |
| | | σ* S16-N19 | 0.23205 | 11.04 | 0.41 | 0.061 |
| LP (3) O17 | 1.78060 | σ* S16-N19 | 0.23205 | 13.21 | 0.52 | 0.074 |
| LP (2) O18 | 1.82021 | σ* C11-S16 | 0.20565 | 16.15 | 0.44 | 0.076 |
| | | σ* S16-N19 | 0.23205 | 10.92 | 0.41 | 0.061 |
| LP (3) O18 | 1.78122 | σ* S16-N19 | 0.23205 | 13.69 | 0.41 | 0.067 |
| LP (1) N19 | 1.92211 | σ* C11-S16 | 0.20565 | 5.33 | 0.49 | 0.047 |

According to Table 8 and Table 9, it is observed that there are interactions between the same donor-acceptor orbitals for VLB and 1H-VLB molecules and the stabilization energies are close to each other.

For example, the stabilization energies for the interactions between the π (N2-C3) donor and the π* (C4-C5) acceptor orbital were calculated as 8.27 kcal/mol for VLB and 9.10 kcal/mol for 1H-VLB. Similarly, another interaction is between π (C4-C5) → π* (N2-C3) orbitals and stabilization energies are calculated as 26.03 kcal/mol for VLB and 24.65 kcal/mol for 1H-VLB. Furthermore, this interaction is the strongest observed for the VLB molecule. For 1H-VLB, the strongest interaction is observed between π (C23-C25) donor orbital (EDi = 1.65380e) and π*(C20-C21) acceptor orbital (EDj = 0.36972e) with stabilization energy of 64.68 kcal/mol. For VLB, E(2) of this interaction was calculated as 21.01 kcal/mol. In addition, the most important lone pair interactions were given in Table 8 and 9 for both molecules.

Table 9. Second-order perturbation theory results of Fock matrix in NBO basis for 1H-VLB

| Donor(i) | $ED_i$/e | Acceptor(j) | $ED_j$/e | $E^{(2)}$ kcal/mol | E(j)-E(i)/a.u | F(i.j)/a.u |
|---|---|---|---|---|---|---|
| σ N2-C3 | 1.98612 | π* C20-C21 | 0.36972 | 7.98 | 0.76 | 0.077 |
| π N2-C3 | 1.89731 | π* C4-C5 | 0.28104 | 9.10 | 0.37 | 0.054 |
| | | σ* S16-O17 | 0.14138 | 9.35 | 0.44 | 0.058 |
| | | π* C20-C21 | 0.36972 | 11.39 | 0.23 | 0.049 |
| π C4-C5 | 1.77906 | π* N2-C3 | 0.31513 | 24.65 | 0.29 | 0.078 |
| | | π* C6-C7 | 0.35105 | 7.41 | 0.31 | 0.044 |
| π C9-C11 | 1.68516 | π* C6-C7 | 0.35105 | 16.72 | 0.30 | 0.064 |
| | | π* C12-C14 | 0.29410 | 20.58 | 0.30 | 0.071 |
| π C12-C14 | 1.65250 | π* C6-C7 | 0.35105 | 21.08 | 0.29 | 0.069 |
| | | π* C9-C11 | 0.38450 | 19.78 | 0.27 | 0.066 |
| π C20-C21 | 1.65008 | π* N2-C3 | 0.31513 | 12.36 | 0.26 | 0.051 |
| | | π* C23-C25 | 0.33041 | 19.83 | 0.29 | 0.068 |
| σ C21-C23 | 1.97641 | σ* S16-O17 | 0.14138 | 21.36 | 0.88 | 0.126 |
| π C23-C25 | 1.65380 | π* C20-C21 | 0.36972 | 64.68 | 0.14 | 0.086 |
| σ C25-H26 | 1.98041 | π* C20-C21 | 0.36972 | 20.29 | 0.44 | 0.093 |
| π C27-C29 | 1.65456 | π* C20-C21 | 0.36972 | 38.80 | 0.14 | 0.066 |
| | | π* C23-C25 | 0.33041 | 20.78 | 0.28 | 0.069 |
| σ C31-O36 | 1.98988 | σ* S16-N19 | 0.23220 | 13.34 | 0.83 | 0.099 |
| σ O36-H37 | 1.98738 | σ* S16-N19 | 0.23220 | 19.95 | 0.49 | 0.094 |
| LP (2) O1 | 1.69685 | π* N2-C3 | 0.31513 | 14.10 | 0.38 | 0.066 |
| | | π* C4-C5 | 0.28104 | 29.77 | 0.40 | 0.098 |
| | | σ* S16-O17 | 0.14138 | 15.76 | 0.47 | 0.080 |
| LP (2) O17 | 1.82000 | σ* C11-S16 | 0.20522 | 16.41 | 0.44 | 0.076 |
| | | σ* S16-N19 | 0.23220 | 11.77 | 0.39 | 0.061 |
| LP (3) O17 | 1.78106 | π* C20-C21 | 0.36972 | 11.43 | 0.19 | 0.043 |
| LP (2) O18 | 1.82016 | σ* S16-N19 | 0.23220 | 21.00 | 0.41 | 0.083 |
| | | π* C20-C21 | 0.36972 | 24.42 | 0.19 | 0.065 |
| LP (3) O18 | 1.78136 | σ* S16-O17 | 0.14138 | 28.43 | 0.39 | 0.096 |
| | | σ* S16-N19 | 0.23220 | 14.30 | 0.39 | 0.067 |

### *Molecular Electrostatic Potential (MEP) Surfaces*

Interpretation of molecular electrostatic potential (MEP) surface maps obtained by quantum chemical methods is seen as one of the effective ways to evaluate the chemical reactivity of a molecule towards positively or negatively charged reagents [45].

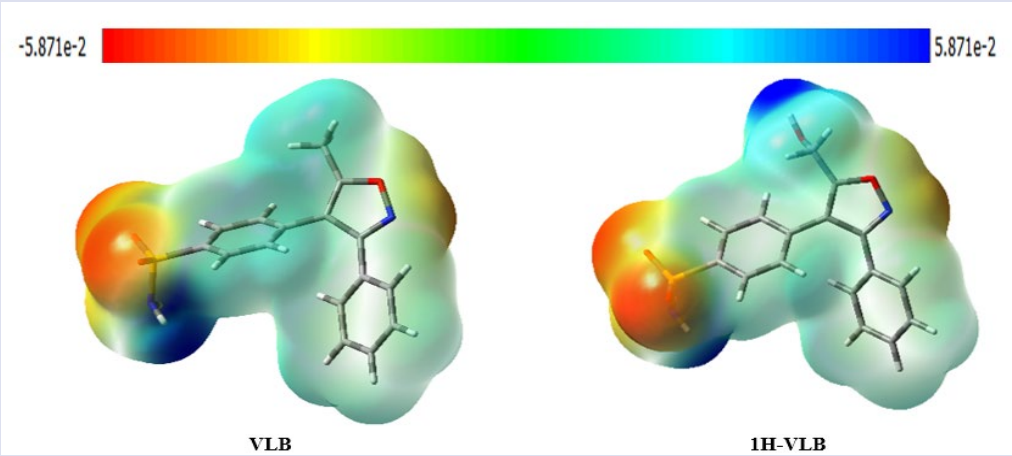


Figure 7. 3D molecular mapped surfaces of studied molecules at B3LYP/6-311++G (d, p) level

Figure 7 shows the MEP maps of studied molecules at B3LYP/6-311++G (d, p) theory level. In 3D charge distribution of MEP, nucleophilic centers are shown in blue, while electrophilic centers are shown in red. The electrostatic potential decreases according to the order blue > green > yellow > orange > red. The MEP maps of the mentioned molecules are in the ranges −0.05871 a. u. (red) and +0.05871 a. u. (blue). From Figure 7, it is seen that the region with the highest electron density is around the oxygen O17 and O18 atoms. On the other hand, the positive regions are the regions where the blue color intensity is the majority on the hydrogen atoms. The N-H and O-H regions show the regions with the lowest electron density.

## Conclusions

In this study, inspired by studies to identify drug candidates with potent and specific anti-inflammatory properties, quantum chemical computations for both vacuum and water phase were performed on valdecoxib and its active metabolite, hydroxy valdecoxib compounds. The results obtained from this research study can be presented as follows:

- Structural parameters calculated at the theory level of B3LYP/6-311++G (d, p) and FT-IR analysis results are in good agreement with the experimental results.
- When the bioactivity of VLB and 1H-VLB molecules were compared based on quantum chemical reactivity identifiers, it was concluded that all parameters except $E_{LUMO}$ supported the conclusion that VLB molecule was more active.
- Molinspiration calculation results indicate that phenyl rings of VLB and 1H-VLB support predominantly lipophilic interactions, and sulfonamide and hydroxyl groups support hydrophilic interactions.
- The changes in atomic charges with the addition of an -OH group to the structure of VLB were investigated by Mulliken population analysis.
- In the next segment, second-order perturbative predictions of interactions between donor-acceptor (bond-antibond) orbitals on the basis of NBO were presented. Accordingly, for VLB, the strongest interaction is observed between π (C4-C5) → π* (N2-C3) orbitals with stabilization energy of 26.03 kcal/mol. On the other hand, for 1H-VLB, the strongest interaction is observed between π (C23-C25) donor orbital (EDi = 1.65380e) and π*(C20-C21) acceptor orbital (EDj = 0.36972e) with stabilization energy of 64.68 kcal/mol.
- From the molecular electrostatic potential maps, it is seen that the regions with the highest electron density are around the oxygen O17 and O18 atoms, while the regions with the lowest electron density are concentrated around the N-H and O-H atoms.

It was concluded that the results obtained from this study are quite compatible with the literature and support each other.

## Acknowledgment

The numerical calculations reported in this paper were fully performed at TUBITAK ULAKBIM, High Performance and Grid Computing Center (TRUBA resources).

## Conflicts of interest

The authors declare that they have no conflict of interest.

## References

[1] Vane J.R., Inhibition of Prostaglandin Synthesis as a Mechanism of Action for Aspirin-like Drugs, *Nature New Biol.*, 231 (1971) 232–235.

[2] Fu J. R., Masferrer J. L., Seibert K., Raz A., Needle-man P., The induction and suppression of prostaglandin H2 synthase (cyclooxygenase) in human monocytes, *J. Biol. Chem.*, 265 (1990) 265 16737-16740.

[3] Battistini B., Botting B., Bakhle Y., SCOX-1 and COX-2:Toward the development of more selective NSAİDs, *Drug News Perspect.,* 7 (1994) 501.

[4] Sayed G., Abou-seri S.M., Kamel G., Moawad M., Celecoxib analogs bearing ben- zofuran moiety as cyclooxygenase-2 inhibitors : design, synthesis and evalua- tion as potential anti-inflammatory agents, *Eur. J. Med. Chem.,* 76 (2014) 482–493.

[5] Abdelall E.K.A., Lamie P.F., Ahmed A.K.M., El-nahass E., COX-1/COX-2 inhibi- tion assays and histopathological study of the new designed anti-inflammatory agent with a pyrazolopyrimidine core, *Bioorg. Chem.,* 86 (2019) 235–253.

[6] Raz A., Wyche A., Siegel N., Needleman P., Regulation of fibroblast cyclooxygenase synthesis by interleukin-1, *J. Biol.Chem.,* 263 (1988) 263 3022-3028.

[7] Wang C., Chen F., Qian P., Cheng J., Recent advances in the Rh-catalyzed cascade arene C–H bond activation/annulation toward diverse heterocyclic compounds, *Org. Biomol. Chem.*, 19 (2021) 1705-1721.

[8] Mermer A., Keleş T., Şirin Y., Recent studies of nitrogen containing heterocyclic compounds as novelantiviral agents: A review, *Bioorg. Chem.,* 114 (2021) 105076.

[9] Zhu Jun J., Hong-zhi M., Yao L., Chen Y., Sun H., The recent progress of isoxazole in medicinal chemistry, *Bioorg. Med. Chem.,* 26 (2018) 3065–3075.

[10] Scheen A.J., Malaise M., Le medicament du mois.Valdecoxib (Bextra), *Rev. Med. Liege*, 59 (2004) 251-254.

[11] Erdelyi P., Fodor t., Varga A.K., Czugler M., Gere A., Fischer J., Chemical and biological investigation of N-hydroxy-valdecoxib:An active metabolite of valdecoxib, *Bioorg. Med. Chem.,* 16 (2008) 5322–5330.

[12] Talley J.J., Brown D.L., Carter J.S., Graneto M.J., Koboldt C.M., Masferrer J.L., Perkins W.E., Rogers R.SShaffer A.F., Zhang Y.Y., Zweifel B.S., Seibert K., 4-[5-Methyl-3-phenylisoxazol-4-yl]-benzenesulfonamide, Valdecoxib: A potent and selective Inhibitor of COX-2, *J. Med. Chem.,* 43 (2000), 775-777.

[13] Van De Waterbeemd H., Gifford E., ADMET in silico modelling: towards prediction paradise?, *Nat. Rev. Drug Discov.,* 3 (2003) 192-204.

[14] Borges R. M., Colby S. M., Das S., Edison A. S., Fiehn O., Kind T., Lee J., Merrill A. T., Merz K. M. Jr., Metz T. O., Nunez J. R., Tantillo D. J., Wang L. P., Wang S., Renslow R. S., Quantum chemistry calculations for metabolomics., *Chem. Rev.*, 121 (2021), 5633–5670.

[15] Genç F, Kandemirli S. G., Kandemirli F., Theoretical B3LYP study on electronic structure of contrast agent ıopamidol, *Acta Chim. Slov.*, 68 (2021) 320-331.

[16] Frisch M.J., Trucks G.W., Schlegel H.B., Scuseria G.E., Robb M.A., Cheeseman J.R., Scalmani G., Barone V., Petersson G.A., Nakatsuji H., et.al., Gaussian 16 Rev. B.01, Wallingford, CT, 2016.

[17] Dennington R., Keith T.A., Millam J.M., GaussView, Version 6 Semichem Inc., Shawnee Mission, KS. 2016.

[18] Becke A.D., A new mixing of Hartree–Fock and local density-functional theories, *J. Chem. Phys.,* 98 (1993) 1372–1377.

[19] Lee C., Yang W., Parr R.G., Development of the Colle-Salvetti correlation-energy formula into a functional of the electron density, *Phys. Rev. B.*, 37 (1988) 785–789.

[20] Becke A.D., Density-functional thermochemistry. III. The role of exact exchange, *J. Chem. Phys*., 98 (1993) 5648–5652.

[21] Marenich A.V., Cramer C.J., Truhlar D.G., universal solvation model based on solute electron density and on a continuum model of the solvent defined by the bulk dielectric constant and atomic surface tensions, *J. Phys. Chem. B.,* 113 (8) (2009) 6378-6396.

[22] Molinspiration Cheminformatics free web services, https://www.molinspiration.com, Slovensky Grob, Slovakia.

[23] Gaillard P., Carrupt P.A., Testa B., Boudon A., Molecular lipophilicity potential, a tool in 3D QSAR: method and applications, *J. Comput. Aided Mol. Des.*, 8 (1994) 83–96.

[24] Koopmans T., Über die zuordnung von wellenfunktionen und eigenwerten zu den einzelnen elektronen eines atoms, Physica, 1(6) (1934) 104-113.

[25] Parr R. G., Pearson R. G.,. Absolute hardness: companion parameter to absolute electronegativity, J. Am. Chem. Soc., 105 (1983) 7512-7516.

[26] Pearson R. G., Absolute electronegativity and hardness correlated with the molecular orbital theory, Proc. Natl. Acad. Sci. U.S.A., 83 (1986) 8440-8441.

[27] Parr R. G., Szentpaly L. V., Liu, S., Electrophilicity Index, J. Am. Chem. Soc., 121 (1999) 1922-1924.

[28] Perdew J. P., Levy M., Physical content of the exact Kohn-Sham orbital energies: band gaps and derivative iscontinuities, Phys. Rev. Lett., 51(20) (1983). 1884-1887.

[29] Perdew J. P., Parr R. G., Levy M., Balduz J. L. Jr., Density functional theory for fractional particle number: derivative discontinuities of the energy, Phys. Rev. Lett., 49 (23) (1982) 1691-1694.

[30] Malathy Sony S. M., Charles P., Ponnuswamya M. N., Yathirajan H. S., Valdecoxib, a non-steroidal anti-inflammatory drug, *Acta Cryst.,* 61 (2005) 108-110.

[31] Kaushal A.M., Chakraborti A.K., Bansal A.K., FTIR Studies on differential ıntermolecular association in crystalline and amorphous states of structurally related non-steroidal anti-ınflammatory drugs, *Molecular Pharmaceutıcs*, 6 (2008) 937–945.

[32] Sundaraganesan N., Ilakiamani S., Salem H., Wojciechowski P. M., Michalska D., FT-Raman and FT-IR spectra, vibrational assignments and density functional studies of 5-bromo-2-nitropyridine, *Spectrochim. Acta A Mol. Biomol. Spectrosc.*, 61 (2005) 2995–3001.

[33] Arıcı K., Vibrational Spectra of 4-hydroxy-3-cyano-7-chloro-quinoline by density functional theory and ab initio Hartree-Fock Calculations, *Int. J. Chem. Technol.,* 1 (2017) 24-29.

[34] Erdoğan M., Serdaroğlu G., New Hybrid (E)-4-((pyren-1-ylmethylene) amino)-N-(thiazol-2-yl)benzenesulfonamide as a potential drug candidate: Spectroscopy, TD-DFT, NBO, FMO, and MEP studies, *ChemistrySelect,* 6 (2021) 9369–938.

[35] Fukui K., Role of frontier orbitals in chemical reactions, *Science*., 218 (1982) 747–754.

[36] Baybas D., Serdaroglu G., Semerci B., The composite microbeads of alginate, carrageenan, gelatin, and poly(lactic-co-glycolic acid): Synthesis, characterization and density functional theory calculations, *Int. J. Biol. Macromol.,* 181 (2021) 322–338.

[37] Sayin K., Üngördü A., Investigations of structural, spectral and electronic properties of enrofloxacin and boron complexes via quantum chemical calculation and molecular docking, *Spectrochim. Acta A Mol. Biomol. Spectrosc.*, 220 (2019)117102.

[38] Brahmia A., Bejaoui L., Rolicek J., Hassen R.B., Serdaroğlu G., Kaya S., Synthesis, crystal structure, Hirshfeld surface analysis and DFT calculations of 2, 2, 2-tribromo-1-(3,5-dibromo-2-hydroxyphenyl)ethanone, *J. Mol. Struct.,* 1248 (2022) 131313.

[39] Blake J. F., Chemoinformatics - predicting the physicochemical properties of 'drug-like' molecules, *Curr. Opin. Biotechnol.*, 11 (2000) 104-107.

[40] Lipinski C. A. ,Lombardo F., Dominy B. W., Feeney,P. J., Experimental and computational approaches to estimate solubility and permeability in drug discovery and development settings, *Adv. Drug Delivery Rev.,* 23 (1997) 3-25.

[41] Mulliken R.S., Electron population analysis on LCAO-MO molecular wave functions, *J. Chem. Phys*., (1955) 1833-1841.

[42] Reed A.E., Weinstock R.B., Weinhold F., Natural atomic orbitals and natural population analysis, *J. Chem. Phys.,* 83 (1985) 735–746.

[43] Weinhold F., Landis C.R., Glendening E.D., What is NBO analysis and how is it useful?, *Int. Rev. Phys. Chem.,* 35 (2016) 399-440.

[44] Reed A.E., Curtiss L.A., Weinhold F., Intermolecular ınteractions from a natural bond orbital, donor-acceptor viewpoint, *Chem. Rev.,* 88(1988) 899-926.

[45] Murray J.S., Politzer P., The electrostatic potential: an overview, *Wiley Interdiscip. Rev. Comput. Mol. Sci.*, 1 (2011) 153-163.